Thermochimica Acta, 78 (1984) 395–421
Elsevier Science Publishers B.V., Amsterdam – Printed in The Netherlands

Review

THERMAL DECOMPOSITION OF TALC: A REVIEW

MAREK WESOŁOWSKI

Institute of Chemistry and Analytics, Medical Academy, Al. K. Marksa 107, Pl 80-416 Gdańsk (Poland)

(Received 6 February 1984)

ABSTRACT

A literature review is presented concerning the application of thermoanalytical methods, such as differential thermal analysis (DTA), thermogravimetry (TG) and derivative TG (DTG) as well as isothermal measurements for the examination of the thermal decomposition of talc. The crystal structure of this mineral is characterized and relations between the talc structure and its physico-chemical properties and thermal stability are given. The usefulness of isothermal and dynamic thermal methods in studies of the mechanism of talc decomposition to cristobalite and magnesium metasilicate, as well as in talc dehydration kinetics is emphasized. Moreover, attention is paid to the interpretation of the shape of endothermic DTA peaks due to dehydroxylation of the mineral, as well as to the possibilities of detection, identification and quantitative determination of the mineral contaminations frequently encountered in talc, such as carbonates, quartz and chrysotile. In a separate chapter, questions connected with the utilization of thermoanalytical curves for the identification of talc, and its distinction from minerals belonging to other groups than the silicate and aluminosilicate classes are discussed.

INTRODUCTION

Talc (talcum, steatite, soapstone, mussolinite) is a natural product, widely used in industry. In cosmetic technology it is used as a cosmetic and a baby powder base, as a cream additive and as a filling material for dyestuffs and soaps [1]. Powdered talc is used as an antiphlogistic agent and as an adsorbent. In the pharmaceutical industry talc is currently applied as a sliding agent [2]. It improves the friability of the tablet mass, and shows an antistatic and antiadhesive action. Moreover, it is used as the component of antiadhesive dusting powder and during coating with lake. Talc has also found wide-spread application in the rubber and the paper industries as a filling material, in the ceramic industry for the production of refractories, and in the manufacture of fireproof paints, high-voltage insulators, and other products [3].

In studies of raw materials, and intermediate and final commercial products containing talc, thermoanalytical methods such as differential thermal

0040-6031/84/$08.10

analysis (DTA), thermogravimetry (TG) and derivative TG (DTG) are mostly applied. This requires knowledge of the thermal decomposition data of talc under dynamic conditions. Knowledge of its mechanism of decomposition and physico-chemical properties may be useful in the detection, identification and quantitative determination of talc.

For the foregoing reasons, it is important to review all data of the thermal decomposition of talc and related problems. This question has not been the subject of a review article as yet, with the exception of Smolin's [4] article published in 1970. The author discusses both major and side thermal effects due to the polymorphism of talc, and specifies the products of its thermal decomposition. He considers their significance for the determination of variations in the mixed-layer composition of the mineral as well as questions related to the stabilization of the properties of products of enstatite ceramics.

CRYSTAL STRUCTURE AND PROPERTIES

From the chemical point of view, talc is magnesium tetrasilicate with a previously ascribed formula $3\ MgO \cdot 4\ SiO_2 \cdot H_2O$. Its crystal structure has been precisely determined with the aid of X-ray crystallography. Silicon oxide tetrahedrons, $[SiO_4]$, are the fundamental structural elements of talc, similar to all other silicates [5–8]. Complexes of the silicon oxide groups form layers of planar lattices in which each tetrahedron shares three corners with the adjacent tetrahedrons. Therefore, three oxygen atoms of each tetrahedron belong simultaneously to two silicon atoms, while the fourth oxygen atom belongs to one tetrahedron only. The ratio of the silicon to oxygen atoms is 2 : 5, thus corresponding to the formula $[Si_4O_{10}]_{\infty}^{4-}$. The charge of the anion layers is counter-balanced by the appropriate numbers of magnesium cations arranged regularly between them as shown in Fig. 1.

From the mineralogical point of view, talc belongs to the class of silicates and aluminosilicates, to the group of talc and pyrophyllite [8]. The formula

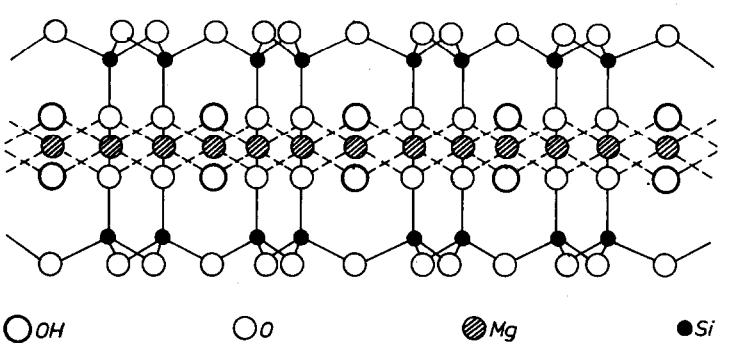

Fig. 1. Crystal structure of talc (from ref. 27).

TABLE 1

Values of the lattice constants in the direction of the crystallographic axes of the unit cell, and values of the β angle for talc

	Gruner [9]	Hendricks [10]	Correns [11]	Zvyagin and Pinsker [12]	Stemple and Brindley [13]
a (Å)	5.27	5.28	5.26	5.27	5.287
b (Å)	9.12	9.12	9.10	9.13	9.158
c (Å)	18.85	18.92	18.81	18.94	18.95
β	100°	100°15′	100°	100°40′	99°30′

$Mg_3[(OH)_2|Si_4O_{10}]$ reflects a simple trioctahedron structure of talc most accurately. There are three-layer packets of the 2:1 type in which the metallo-hydroxyl layer is sandwiched between two layers of silicon oxide anions, facing each other with their active surfaces. The structure of this type is characterized by almost completely compensated, stable and strong bonds.

Talc is characterized by the high symmetry of the unit cell. It crystallizes in the monoclinic system, space group C_{2c} or C_c. Hexagonal crystals are encountered very rarely. The values of the lattice constants in the directions of the crystallographic axes of the unit cell, and the values of the β angle for talc, are compiled in Table 1 [9–13].

Lindemann et al. [14] showed that Austrian talc crystallizes in the triclinic system, space group P_1. The values of the lattice constants in the direction of the crystallographic axes are $a_0 = 5.32$, $b_0 = 9.17$ and $c_0 = 9.46$ Å, and the value of the β angle is 94.0°. Somewhat different values of the lattice constants showed by other authors may be due to the presence of contaminants, such as Fe^{2+}, Cr^{3+} or F^- ions.

The crystal structure of talc is reflected in some physical properties [5–8]. Its layer structure gives excellent cleavage in the direction of the plane of the silicon oxide anions. This is due to the weak interactions of the van der Waals bonds between the packets. The softness of talc is also due to the ease of displacement of these layers. Moreover, talc is a bad electrical and thermal conductor. It is a refractory, resistant to acids. Talc is a fatty substance to the touch.

CRYSTAL STRUCTURE AND STABILITY

The symmetry of the crystal structure of silicates and aluminosilicates has a great influence on their thermal stability. According to Kiefer [15], the dehydration temperature range of some layer minerals is directly related to the symmetry of the crystal lattice within a given lattice type, and to the

symmetry of the valence bonds within the octahedral layer. Thus, minerals whose cations are slightly larger than the spaces left by the oxygen atoms in the octahedral layer have maximum stability. These facts can be summarized by empirical relationships which enable the prediction of the existence of several minerals not previously identified, their zones of dehydration, and the shape of the dilatation or shrinkage curves.

Thermal stability of the silicates also increases with increasing symmetry of the layers and with an increase in centrally located hydroxyl groups [16]. Kaolinite serves as an example. It is a layer aluminosilicate represented by the formula $Al_4[(OH)_8|Si_4O_{10}]$, belonging to the group of kaolinite and serpentine. Part of its hydroxyl groups are located at the surface of the layers. Compared with talc, it is less stable because the hydroxyl groups of talc are located inside the crystal lattice. The thermal stability of minerals also increases with an increase in the number of cations neutralizing the charge of the anionic layers. Silicates having octahedral configuration with six cations, e.g., talc (6 Mg^{2+}), are more stable compared to those having only four cations, e.g., pyrophyllite (4 Al^{3+}). Pyrophyllite is a layer aluminosilicate represented by the formula $Al_2[(OH)_2|Si_4O_{10}]$, belonging to the group of talc and pyrophyllite.

Furthermore, the thermal stability of silicates and aluminosilicates also increases with increasing symmetry of the bonding and with ionic density in the octahedron [16]. It attains a maximum when the central cation is surrounded by six oxygen anions. This is due to the fact that the value of the coordination number is a function of the radius of cation and of the deformation of the oxygen anions. Because the ionic radius of both Mg^{2+} and Ni^{2+} is 0.78 Å, the thermal stability of minerals containing them is equal. However, the stability is decreased with minerals containing Mn^{2+} ions due to its greater ionic radius (0.91 Å).

Systematic dilatometric studies of the layer silicates and aluminosilicates performed by Kiefer [17] showed that the general shape of the dilatation–shrinkage curves may be related to the crystal structure of these minerals, their texture and mechanical changes in the structure observed on a macroscopic scale. Temperature zones and amplitude of the dilatometric anomalies are connected with the decomposition of the mineral by dehydration, recrystallization of the thermal decomposition products, and fusion of the constituents of the reaction mixture. The temperature zones in which the reactions take place depend on factors affecting the thermal stability of minerals, e.g., the structure of the crystal lattice and saturation of the octahedral layer, as well as on the chemical nature of the constituents. The textural and mechanical changes in the structure of minerals affect the reactions of recrystallization and fritting. It must be noted that the shape of recorded curves depends much on the grinding of a sample and its moulding.

THERMAL DECOMPOSITION

Talc contains adsorption water and water in the form of hydroxyl groups which constitutes the space lattice elements [18]. During the heating of the mineral, water is liberated in distinct steps due to differences in its bonding energy. An endothermic DTA peak due to the loss of the adsorption water occurs at 373–773 K, on the other hand, exothermic effects at higher temperatures can be ascribed to the splitting of the constitution water.

Ewell et al. [19] reported that the adsorption water of talc is mostly driven off between 653 and 773 K and is accompanied by a small endothermic DTA effect, but not by any change in the crystal structure or optical properties of the mineral. On the other hand, one mole of the constitution water is driven off between 1073 and 1123 K. This water loss is accompanied by a large endothermic DTA effect.

Avgustinik et al. [20,21] observed three stages of talc dehydration at 393–473, 623–773 and 873–1323 K. During the third stage of the mineral dehydration, 5.1% total nonhygroscopic water is liberated. The remaining 0.4% water is liberated during the first two stages of dehydration. It is not accompanied by the breakdown of the crystal structure of the mineral. The adsorption water is distributed between the basal surfaces of the packets and within the packets of the crystal structure of talc.

After the second, great endothermic peak, an exothermic effect is usually observed due to the crystallization of silica as cristobalite, and crystallization of magnesium metasilicate [18]. In the identification of the crystalline dehydration products, X-ray diffraction analysis is very useful.

Thilo and Rogge [22], and Stone [23] showed that the liberation of the constitution water is accompanied by the decomposition of talc into free magnesium oxide and silica. Heating the reaction mixture to 1273 K leads to the formation of crystalline phase M_1 which, above 1273 K, converts to crystalline phase M_2 [22]. Up to 1523 K it transforms into mesoenstatite which, as a result of a further increase in temperature, becomes clinoenstatite. This is illustrated by the following scheme

$$\mathrm{Mg_3[(OH)_2|Si_4O_{10}]} \xrightarrow{1223\ \mathrm{K}} \underset{\text{(amorphous oxides)}}{3\ \mathrm{MgO} + 4\ \mathrm{SiO_2} + \mathrm{H_2O}} \tag{1}$$

$$3\ \mathrm{MgO} + 4\ \mathrm{SiO_2} \xrightarrow{<1273\ \mathrm{K}} M_1 \xrightarrow{>1273\ \mathrm{K}} M_2 \tag{2}$$

$$M_2 \xrightarrow{>1373\ \mathrm{K}} \underset{\text{(protoenstatite)}}{\mathrm{MgSiO_3}} + \underset{\text{(amorphous)}}{\mathrm{SiO_2}} \tag{3}$$

$$\mathrm{MgSiO_3} + \mathrm{SiO_2} \xrightarrow{>1523\ \mathrm{K}} \underset{\text{(clinoenstatite)}}{\mathrm{MgSiO_3}} + \underset{\text{(cristobalite)}}{\mathrm{SiO_2}} \tag{4}$$

These authors [22] concluded that enstatite is stable to temperatures below

1173 K, protoenstatite between 1173 and 1523 K, and clinoenstatite is stable above 1523 K.

Lindemann [24–26] also showed that the dehydroxylation at 1123 K leads to the formation of protoenstatite and amorphous silica. He found that the crystal structure of protoenstatite was very close to the talc structure. When talc is dehydroxylated, two hydroxyl groups produce a molecule of water, but the remaining O^{2-} ion displaces within the crystal lattice to form Si–O–Si bridges. This causes the silicon oxide tetrahedra, $[SiO_4]^{4-}$, to form a chain thus transforming the layer structure of talc into the chain structure of protoenstatite. Up to 1723 K, protoenstatite converts to clinoenstatite, whereas silica crystallizes as cristobalite.

Krönert et al. [27] preceded studies on the thermal decomposition of talc and the stability of the crystal modifications of magnesium metasilicate by an exhaustive literature review. It has been shown that the dehydroxylation of talc starts at 1073 K in air, whereas in vacuum the process begins at 973 K [28,29]. This leads to the formation of protoenstatite and amorphous silica. At 1373 K it transforms to cristobalite. The presence of mineralizers speeds up the process of talc decomposition and the formation of new crystals [28]. On the addition of lithium fluoride talc changes, via clinoenstatite and amphibole containing fluorine, into enstatite and quartz. The influence of mineralizers on the dehydroxylation of talc is illustrated in Fig. 2. Annealing of the talc glass leads to protoenstatite via clinoenstatite. As a result of rapid cooling of the reaction mixture, protoenstatite transforms to clinoenstatite [28,29]. This can also be performed mechanically, e.g., by grinding or compressing. It has also been established that protoenstatite is a modifica-

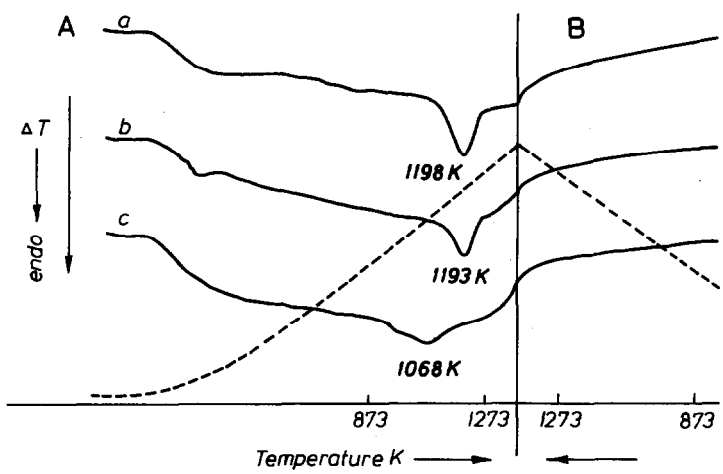

Fig. 2. DTA curves of the thermal decomposition: (A) heating, and (B) cooling, of (a) Stemag talc and its samples containing: (b) 2% boric oxide, and (c) 2% lithium fluoride (from ref. 28). Measurements were performed at a heating rate of 10 K min^{-1}. Samples were powdered to < 60-μm particle size.

tion which is stable at higher temperatures, while clinoenstatite is not so stable; it is the metastable form at each temperature.

X-ray diffraction analysis of talc obtained from a sample heated to various temperatures indicated that talc heated to 1268 K shows a small amount of protoenstatite [30]. This is confirmed by the X-ray patterns. At 1335 K diffraction lines corresponding to talc disappear and all the remaining lines confirm the presence of protoenstatite. At 1573 K the strongest diffraction line of α-cristobalite appears. Furthermore, when the sample was heated for longer at this temperature, an increase in the intensity of the diffraction line of α-cristobalite was found. From these results, Ishii et al. [30] concluded that the thermal decomposition of talc to protoenstatite begins rapidly at about 1173 K, with the formation of protoenstatite (Fig. 3).

A different opinion on the dehydroxylation of talc has been presented by Ewell et al. [19]. In their opinion, the decomposition of talc is accompanied by the formation of enstatite and amorphous silica. The inversion of enstatite to clinoenstatite takes place gradually, both phases being observed in the material heated at 1473 K. The presence of clinoenstatite alone has been detected at temperatures as high as 1573–1708 K. Simultaneous with the observed changes, the transformation of amorphous silica to cristobalite took place. It is illustrated by the following scheme

$$Mg_3[(OH)_2|Si_4O_{10}] \xrightarrow{1073\ K} \underset{\text{(enstatite)}}{3\ MgSiO_3} + \underset{\text{(amorphous)}}{SiO_2} + H_2O \qquad (5)$$

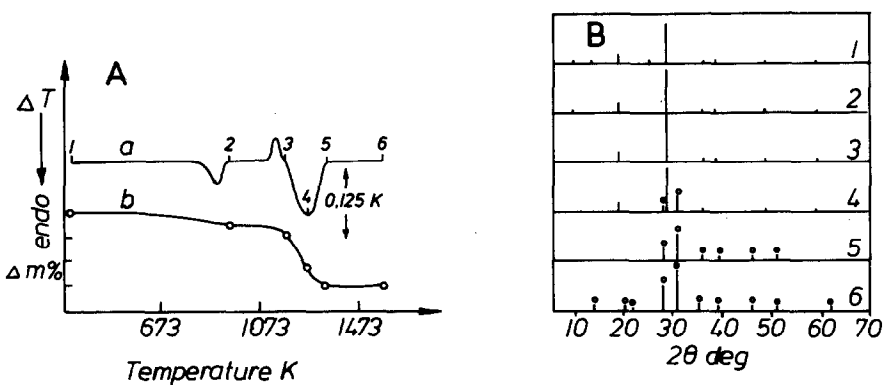

Fig. 3. (A, a) DTA, and (b) TG curves of the talc thermal decomposition (from ref. 30). DTA instrument by Rigaku (model 8001) and TG apparatus consisted of a quartz spring with a sensitivity of 3.25×10^{-3} g min^{-1} were used. Samples (300 mg) were heated at a rate of 10 K min^{-1} in a static air atmosphere, and α-Al_2O_3 was used as reference material. Samples were powdered to 300-mesh particle size. (B) X-ray diffraction pattern of the samples obtained heated to various temperatures denoted by Arabic numbers on the DTA curve: (1) 298 K, (2) 933 K, (3) 1163 K, (4) 1268 K, (5) 1335 K, and (6) 1573 K. Designations on the diffraction patterns: (○) protoenstatite, (●) α-cristobalite, and (no mark) talc. Measurements were performed using a Geigerflex X-ray diffractometer (model 2141).

$$3\ MgSiO_3 + SiO_2 \xrightarrow{1573\ K} \underset{\text{(clinoenstatite)}}{3\ MgSiO_3} + \underset{\text{(cristobalite)}}{SiO_2} \quad (6)$$

The presence of the metaphase, or protoenstatite, has not been ascertained amongst the decomposition products. This is in agreement with the DTA and X-ray studies of Planz [31]. Below 1323 K, neither protoenstatite nor clinoenstatite has been found in the decomposition products. Just above this temperature enstatite and amorphous silica have been identified. At higher temperatures silica crystallizes as cristobalite, whereas at 1473 K enstatite converts into the high-temperature crystal modification, protoenstatite.

When studying the solubility of the decomposition products of talc in hydrochloric acid and sodium hydroxide solutions, Avgustinik et al. [20,21] showed that free magnesium oxide was formed in a negligible amount only. Above 873 K regrouping of the ions within the lattice of the non-decomposed talc begins. Part of the amorphous silica is split from the talc within the optimum temperature interval for this reaction (1023–1123 K) [20]. The remaining part of the silica is bonded with magnesium oxide in the form of amphibole-like double-chain fragments of the crystal lattice of talc which form an independent γ-phase [21]. This is due to the fact that bonds between the Mg^{2+} ions and the $[SiO_4]^{4-}$ tetrahedrons in the crystal lattice of talc are ruptured faster than bonds between the Mg^{2+} ions and the OH^- groups [20]. After rupture of these bonds, a portion of the constitution water remains in the crystal lattice of the mineral.

Over the temperature interval 1273–1473 K, the amphibole double chains are also gradually broken down to form pyroxene-like metasilicate chains [21]. Moreover, free amorphous silica crystallizes as cristobalite. Between 1523 and 1623 K, the chains of the pyroxene-like β-phase attain an improved ordering to form distinct clinoenstatite chains, and the needle-like shape of the crystals becomes dominant. The structure of this clinoenstatite α-phase is initially still rather defective, and includes many cavities in the cell structure. This is shown in the scheme

$$\text{Talc} \xrightarrow{873\ K} \gamma\text{-phase} \xrightarrow{1273\ K} \beta\text{-phase} \xrightarrow{1473\ K} \text{clinoenstatite} \quad (7)$$

The symmetry of the γ-phase is assumed to be that of the orthorhombic system in which half of the initial hydroxyl groups of the talc structure is present. On the other hand, the β-phase is referred to as an anhydrous amphibole which crystallizes in a monoclinic system. In the crystallographic relation of the initial talc to the γ-phase, the change of the *c* and *a* axes to the reversed orientation is characteristic.

Bošković et al. [32] showed that at 973 K talc does not undergo any structural transformation although the dehydration process has already started (Fig. 4). At 1223 K the crystal structure of the mineral starts to decompose and becomes disordered. The presence of enstatite has been confirmed in the decomposition products. This is illustrated by the weight

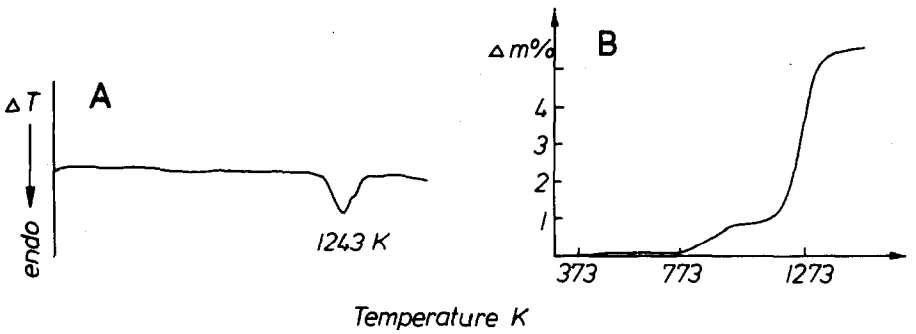

Fig. 4. (A) DTA, and (B) TG curves of the thermal decomposition of SVC Italian talc (from ref. 32). Measurements were performed using an R.L. Stone DTA instrument, at a heating rate of 10 K min^{-1}. 60–100-μm fractions were used.

loss on the TG curve and the endothermic DTA peak at 1243 K. A completely new crystal structure of the clinoenstatite is formed at 1573 K. In addition, enstatite and protoenstatite were also found in the reaction mixture.

The process of the dehydroxylation of talc to form enstatite has been elucidated by Dereń et al. [33]. They showed that the reaction can be formally written as follows

$$Mg_6Si_8O_{20}(OH)_4 \rightarrow 6\ MgSiO_3 + 2\ SiO_2 + 2\ H_2O \tag{8}$$

Relations between the dimensions and the spatial orientation of interconverting structures of talc and enstatite are simple and can be represented by the following set of equations

talc		enstatite
a	= 5.29 Å	$\approx c =$ 5.18 Å
b	= 9.16 Å	$\approx b =$ 8.81 Å
$d(001)$	= 18.70 Å	$\approx a =$ 18.23 Å

(9)

From these equations it follows that one unit cell of talc, containing the following number of atoms: 12 Mg, 16 Si, 48 O and 8 H, converts to one unit cell of enstatite comprising 16 Mg, 16 Si and 48 O.

In a specified volume in which talc converts into enstatite, the number of the silicon and oxygen atoms remains unchanged. This is in agreement with the ordered transition of the silicon oxide fragment of talc to enstatite. This relation is not described by a formalistic equation of the chemical reaction. In reality, this transition comprises the loss of eight protons from the considered volume. It is compensated by supplying a charge equivalent to the appropriate number of the magnesium ions (four). Although talc is a layer silicate, while enstatite is a chain silicate, the oxygen and silicon ions of the silicon oxide layer of talc practically remain in their former positions.

The reaction requires only a slight displacement of the cations within the fragment representing the magnesium–oxygen–hydrogen layer.

On the margin of these problems, works of Koltermann [34–36] should be mentioned. He examined the decomposition of talc in the presence of lithium fluoride as mineralizer. Moreover, Pistorius [37], and Kitahara et al. [38] studied some phase relations of the system $MgO–SiO_2–H_2O$ under high-temperature and high-pressure conditions. This type of study is helpful in the explanation of the formation of talc under natural conditions.

DEHYDRATION KINETICS

The dehydration of talc is a typical example of a solid-state reaction. As a result of this reaction, new solid and gaseous products are formed. Taking into account the significance of the mineral as a raw material in ceramic manufacture, the knowledge of its dehydration kinetics is particularly important.

Avgustinik and Sverchkova [39] examined the dehydration of onotski talc under isothermal conditions. Powdered mineral samples (900 mesh) were heated in an oven at 673–1273 K. Analysis of the results showed that dehydration rate constants were best described by Jander's equation [40]

$$\left[1-(1-\alpha)^{1/3}\right]^2 = k_J t \tag{10}$$

where k_J is the rate constant of the reaction ($k_J = -kDr^{-2}$), α is the reaction rate, D is the diffusion coefficient, r is the radius of the spherical particle, and t is the time.

Dehydration rate constants of talc are compiled in Table 2. Their graphical interpretation as a plot of $\log k_J = f(T)$, shows that mineral dehydration occurs in three stages:

(I) below 873 K, characterized by a constant temperature coefficient

TABLE 2

The rate constants of dehydration of the onotski talc [39]

Temp. (K)	$1/T \times 10^{-4}$	k	$\log k$	$\ln k$	Constant temp. coefficient
673	14.8	1.1×10^{-5}	−4.96	−11.41	4.8
773	12.93	5.3×10^{-5}	−4.28	−9.84	4.5
873	11.4	2.4×10^{-4}	−3.62	−8.33	8.3
973	10.2	2.0×10^{-3}	−2.70	−6.21	11.0
1073	9.3	2.2×10^{-2}	−1.66	−3.82	3.8
1173	8.5	8.4×10^{-2}	−1.08	−2.48	1.6
1273	7.8	1.3×10^{-1}	−0.87	−2.00	

(approximately 4.6 times per 100°);

(II) between 873 and 1073 K, characterized by an increasing temperature coefficient which attained a maximum value at 1073 K;

(III) observed above 1073 K, described by a decreasing temperature coefficient. The highest loss of water was observed between 1073 and 1273 K.

The activation energies of stages (I) and (II) of the mineral dehydration were calculated on the basis of the Arrhenius equation [39]

$$\ln k = \frac{E_a}{RT} + C \tag{11}$$

where E_a is the activation energy, R is the gas constant, T is the temperature (K), and C is a constant.

Graphical presentation of the equation

$$\ln k = f\left(\frac{1}{T} \times 10^{-4}\right) \tag{12}$$

gave the following expressions for the dehydration stages (I) and (II)

$$\ln k_I = -0.905\frac{1 \times 10^4}{T} + 1.99 \tag{13}$$

$$\ln k_{II} = -2.13\frac{1 \times 10^4}{T} + 15.99 \tag{14}$$

By relating eqns. (13) and (14) to eqn. (11), the following mathematical forms were obtained

$$\frac{E_a^I}{RT} = \frac{0.905 \times 10^4}{T} \tag{15}$$

$$\frac{E_a^{II}}{RT} = \frac{2.13 \times 10^4}{T} \tag{16}$$

From transformations (15) and (16), the activation energy was calculated for stage (I) of the mineral dehydration as 18 kcal mol^{-1}, and for stage (II) as 42.3 kcal mol^{-1}. The magnitude of the activation energy gave indirect information about the nature of bonding of the water in talc.

By applying Rengo's equation (eqn. 17), determining the enthalpy of the saturated vapour obtained by evaporation of one mole of water in droplet form, the activation energy for dehydration stage (I) of talc was calculated to be 14.2 kcal mol^{-1}

$$Q = (606.5 + 0.305t) \times 18 \tag{17}$$

where Q is the enthalpy of saturated water vapour, t is the final temperature of stage (I) of dehydration, and 18 is the molecular weight of water.

On the basis of these calculations, it was concluded that water lost in dehydration stage (I), constituting about 6–7% of the total water content of

the mineral, is present in a free form. The remainder, requiring a 2.5 times greater activation energy, was bound in the crystal lattice in the form of hydroxyl groups.

Bošković et al. [41] completed and confirmed the above studies. These authors examined a polydispersed powder of an SVC Italian talc containing only fractions 60–100 μm in diameter. It was found by TG analysis that the total amount of water was 5.54%, of which 0.3% was the hygroscopic moisture as water in a molecular state, while the rest was constitution water.

Data obtained from the examination of talc under isothermal conditions between 673–1373 K were analysed by applying the Jander [40], Gistling and Brounstein [42], and Dünwald and Wagner [43] equations. It is apparent that in the derivation of the Jander equation the dependence of diffusion in spheric bodies was not taken into account. Moreover, the decrease in chemical potential of a diffusing elementary particle was approximated to a straight line. Gistling and Brounstein [42] justifiably abandoned the linear approximation of the decrease in chemical potential along the reaction layer and derived the following equation according to the actual change in the chemical potential

$$1 - \tfrac{2}{3}\alpha - (1-\alpha)^{2/3} = k_G t \tag{18}$$

where k_G is the rate constant of the reaction.

A dependence between the rate constant and time is described by Fick's second law. On the basis of this relation, Dünwald and Wagner [43] obtained the following equation

$$1 - \alpha = \frac{6}{\pi} \sum_{n=1}^{\infty} \frac{1}{n^2} \exp\left(-n^2 k_W t\right) \tag{19}$$

where k_W is the rate constant of the reaction ($k_W = -\pi D r^{-2}$), and n is a whole number.

Average values of the rate constants of the dehydration of talc were calculated on the basis of eqns. (10), (18) and (19). They are compiled in Table 3. Their graphical presentation as $\log k = f(1/T)$ shows that the dehydration is a two-stage process. Stage (I) occurs up to 1023 K while stage (II) is from 1023 to 1323 K. From the slope of the straight lines the corresponding activation energies were obtained. They are compiled in Table 4.

Assuming that 1023 K denotes the final temperature of stage (I), the activation energy calculated from the Rengo equation (eqn. 17) is 15.1 kcal mol^{-1}. Consequently it follows that 5–6% of the total amount of water is liberated from talc in the first dehydration stage.

Bošković et al. [41] also showed that the use of the equation derived by Jordan–Duwez [44] enables the calculation of more precise values of the activation energy

TABLE 3

Average values of dehydration rate constants of the SVC Italian talc [41]

Temp. (K)	$1/T \times 10^{-4}$	k_J	k_G	k_{DW}
665	15.02	5.52×10^{-5}	7.42×10^{-5}	2.24×10^{-4}
783	12.79	3.49×10^{-4}	2.82×10^{-4}	2.43×10^{-3}
973	10.30	2.24×10^{-3}	2.19×10^{-3}	1.56×10^{-2}
1073	9.30	4.78×10^{-3}	4.53×10^{-3}	3.57×10^{-2}
1123	8.90	2.74×10^{-2}	1.88×10^{-2}	0.154
1173	8.50	5.88×10^{-2}	4.68×10^{-2}	0.401
1223	8.16	1.32×10^{-1}	0.95×10^{-1}	0.876
1273	7.85	2.57×10^{-1}	1.66×10^{-1}	1.634
1323	7.55	4.16×10^{-1}	2.30×10^{-1}	2.608
1373	7.26	6.97×10^{-1}	2.54×10^{-1}	3.170

$$\frac{1}{t} = \frac{1}{t_0} \exp\left(-\frac{E_a}{RT}\right) \tag{20}$$

In this equation the polydispersity of the sample does not affect the calculation. The activation energy value of the second dehydration stage of talc is 50 kcal mol^{-1}.

The kinetics of reaction are also characterized by the reaction order. Some authors [45–50] pointed out that the two-stage process of the dehydration obeyed first-order kinetics for more than 90% of the reaction. The temperature intervals and the activation energy values for particular stages of the mineral dehydration, calculated by means of isothermal TG measurements, are in good agreement with the previously cited communications [46–50].

Kinetic parameters of the talc dehydration also depend to a certain degree on various factors other than the chemical composition of mineral. Usov and Sobora [48] showed that the constant temperature coefficient at 1173 K for the second dehydration stage of the onotski talc is 0.368 min^{-1} while for the alguiski talc it is 0.263 min^{-1} at the same temperature. The cited studies [45,48,49] confirm beyond any doubt that the problem of the mechanism of the talc dehydration is governed by structural changes taking place on heating.

TABLE 4

Activation energy of dehydration of the SVC Italian talc [41]

Equation	E_a^I (kcal mol^{-1})	E_a^{II} (kcal mol^{-1})
Jander [40]	14.9	39.74
Gistling–Brounstein [42]	14.2	40.71
Dünwald–Wagner [43]	14.7	39.70

INTERPRETATION OF THERMOGRAMS

In the mineralogical studies, the thermoanalytical methods enable qualitative and quantitative estimation of the mineral composition of a substance of natural origin [18]. The DTA method gives results which enable the deduction of the composition of the mineral phase. On the other hand, the TG method enables the determination of the weight loss at a particular temperature interval. Simultaneous DTA–TG measurements constitute a valuable contribution to the quantitative chemical analysis which is used to estimate the total chemical composition of a sample. Due to the requirement of a small sample size and the possibility of relatively fast determination, thermoanalytical methods are especially valuable in the routine analysis of mineral samples.

Theoretically, talc contains 63.35% SiO_2, 31.90% MgO and 4.75% H_2O. It must be noted that talc minerals occurring in nature are rarely chemically pure substances. Frequently, depending on the geochemical conditions, minerals differing in chemical composition appeared in the different deposits, containing distinct contaminations in the crystal lattice. This is shown in Table 5 in which the chemical composition of talc samples of different origin are shown. As is seen from Table 5, particular minerals have a composition deviating more or less from the theoretical one.

For the foregoing reasons, the DTA and TG curves of the thermal decomposition of the various samples of the mineral differ from each other, depending on the origin and preliminary preparation of the sample. These dissimilarities are especially evident between 673 and 1173 K.

TABLE 5

Chemical composition (wt%) of the talc samples of different origin

	Göpfersgrün [27]	Mautern [27]	China [27]	Rhode Island [27]	Stemag [28]	Italy [32]	U.S.S.R. [39]
SiO_2	63.32	62.93	62.30	61.75	58.00	60.05	61.36
Al_2O_3		4.02	0.06		1.47	3.91	0.72
FeO		0.76	1.62	1.70			
Fe_2O_3	0.57				1.86	1.89	1.46
CaO		1.07			0.70	0.68	1.90
MgO	31.49	30.76	31.32	31.68	31.35	27.54	29.41
K_2O					0.02	0.51	
Na_2O					0.11	0.21	0.87
H_2O	4.38	2.72	4.89	3.83	5.37	5.54	5.17

INTERPRETATION OF THE SHAPE OF AN ENDOTHERMIC DTA PEAK

A DTA curve of talc displays only one major endothermic peak due to dehydroxylation which frequently occurs in the region 1223–1273 K [51]. The shape of this peak can yield useful information concerning the atomic composition of the crystal lattice of the mineral. The appearance of this peak as an unresolved doublet suggests isomorphic substitution in the crystal lattice [52]. It is hypothesized that the variation in the bond strength, which is due to the presence of the isomorphically substituted ions, e.g., nickel or iron, can contribute to the second mode of energy absorption during degradation of the crystal structure. This energy is responsible for the appearance of the endothermic doublet.

Stoch and Stoch [53–55] offered the differentiation of the DTA curves when analysing the shape of the DTA endothermic peaks. This is based on plotting spacings between subsequent points of the endothermic effect as a function of the time of duration of the measurement, or the temperature of the sample. To eliminate the relationship between the amplitude of the differential DTA curve and the magnitude of endothermic effect, it is convenient to use a relative value

$$\left| \frac{\mathrm{d}\left(\frac{\Delta T}{\Delta T_{\mathrm{m}}} \right)}{\mathrm{d}t} \right| = f(t) \tag{21}$$

where ΔT is the spacing between subsequent points on the DTA curve, ΔT_{m} is the effect amplitude on the DTA curve, and t is the time of duration of the measurement.

A differential curve with two branches in one direction is obtained, because the sign of differentiation is omitted. This is illustrated in Fig. 5. The differential curves plotted in this way enable comparison of the left- and the right-hand sides of the DTA effect, and to compare the DTA peaks with each other. The comparison of the shape of both branches of the differential DTA curve characterizes the peak shape whereas a shape index is equal to the ratio of the height of both branches

$$s = \frac{a}{b} = \frac{\Delta(\Delta T)_{m_1}}{\Delta(\Delta T)_{m_2}} \tag{22}$$

where s is the shape index. Amplitudes of the differential DTA curve, a is the left and b is the right branch. The largest spacing between successive points of the endothermic DTA peak, $(\Delta T)_{\mathrm{m}_1}$ is the left- and $(\Delta T)_{\mathrm{m}_2}$ is the right-hand side of the peak.

The endothermic effect of the dehydroxylation of talc usually exhibits a symmetric peak with the shape index around 1.0 [53]. When the DTA peak is a superposition of two neighbouring effects, it is clearly reflected on the

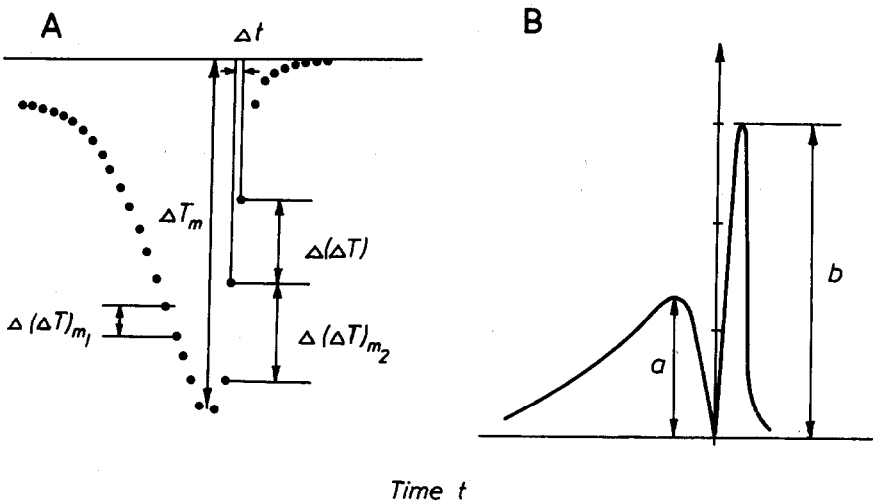

Fig. 5. (A) Construction method of the shape index on the basis of the DTA scanning curve (from ref. 53). (B) Differential DTA curve.

differential curve because one of the branches has a two-humped shape. This causes a change of the shape index of this peak [53–55]. Its value can also be used in the identification of the mineral and in the quantitative determination of its composition [55].

DETECTION AND DETERMINATION OF MINERAL CONTAMINATIONS

The shape of the DTA curve of talc can also give information on the water and the trace quantities of contaminations contained in talc [51]. Identification of the corresponding thermal transitions can be achieved directly by the addition of small quantities of these mineral impurities to the analysed talc sample. DTA coupled with supporting X-ray diffraction analysis is sufficient to positively identify trace contaminations present in the mineral.

Ewell et al. [19] attributed the presence of a minor endothermic DTA peak in the temperature region 773–823 K to the loss of water which is held electrostatically between the basal cleavage planes of the talc crystal. Water bound in this manner would be liberated at a temperature higher than that of adsorbed water but at a lower temperature than that which is bound by the crystal lattice of talc.

Pask and Warner [52], when observing the behaviour of different kinds of talc during heating, noticed that an endothermic DTA effect below 1223 K reflects the decomposition of the carbonate contaminations. This is due to the evolution of carbon dioxide during the thermal decomposition of magnesium or calcium carbonates. DTA is particularly sensitive for the detection

of these minerals. Levels less than 0.5% by weight can be detected by characteristic thermal peaks.

Andreev [56] showed that the thermal decomposition of magnesium carbonate is reflected on the DTA curve of talc as an endothermic effect between 873 and 1073 K. On the other hand, there is an exothermic effect around 1173 K due to the oxidation of ferrous oxide to hematite. These reactions explain the cracking of bricks and plates on firing which had been manufactured by using talc carbonate rocks as a raw material. Thermal effects on the DTA curves of the talc rocks due to oxidation of iron were also observed by Gawel [57].

Schelz [58,59] showed that DTA appears to be a reasonably sensitive, specific and relatively rapid technique for the detection of small amounts of free crystalline quartz in clay minerals. The method utilizes the thermal transition representing the reversible α to β crystal inversion of quartz at 846 K. The latent heat of inversion gives rise to an endothermic effect on the DTA curve of heating. The measurements are preceded by the calcination of a sample at approximately 1073 K for the purpose of inducing irreversible thermal transitions characteristic of that mineral and its impurities. The cooling curve then shows a flat baseline thus improving detectability of quartz in the talc sample.

The minimum level of the detection of quartz in cosmetic talc samples is 0.5% [58]. This is illustrated in Fig. 6A. The endothermic peak at 803 K is due to the decarboxylation of magnesite whereas the next peak is due to the decarboxylation of dolomite or the mixture of dolomite and calcite. The

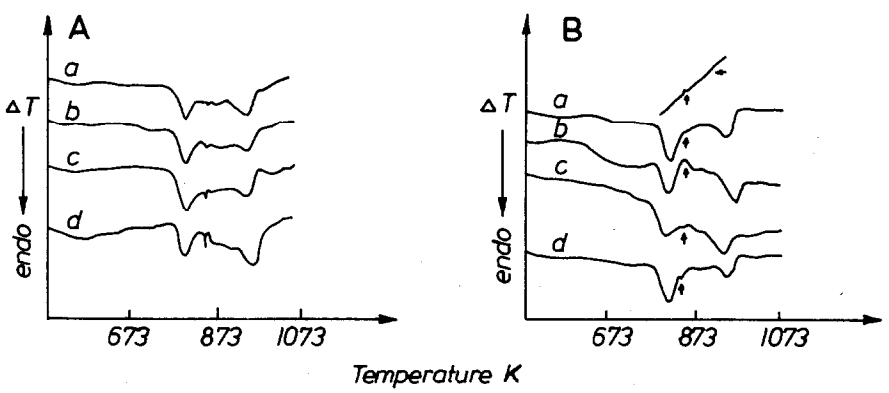

Fig. 6. (A) DTA curves of the thermal decomposition of the cosmetic talc samples containing: (a) 0.5%, (b) 1.0%, (c) 2.0%, and (d) 5.0% standard quartz (from ref. 58). (B) DTA curves of the thermal decomposition of the cosmetic talc samples containing 1.0% standard quartz of various particle size distribution: (a) < 2 μm, (b) < 8 μm, (c) 8-12 μm, and (d) < 12 μm. On the cooling curve the thermal transition for quartz of less than 2-μm particle size was shown. Measurements were performed using an R.L. Stone DTA (model RC-202C) instrument. Samples (150 mg) were heated at a rate of 10 K min^{-1} in a static air atmosphere, and Al_2O_3 was used as reference material. All samples were of 325-mesh particle size.

influence of the particle size distribution of crystalline quartz on its detectability is shown in Fig. 6B. As indicated, the thermal transition for quartz of less than 2-μm particle size was difficult to detect on the heating curve. It is only slightly more evident on the cooling DTA curve.

In the quantitative determinations of the quartz content in talc samples and industrial dusts, Weiss et al. [60–63] used the height of an endothermic DTA peak of the quartz crystal inversion. Analytical accuracy of the determinations by this method depends on the knowledge and control of the variables affecting the DTA response, especially the particle size distribution of the quartz crystal fractions in the samples, the thermal conductivity difference between the inert reference and sample, and the means of sample packing in the crucible [61].

A distinct decrease in the height of the endothermic DTA effect was observed with decreasing particle size of quartz diluted with silicon carbide. This is shown in Fig. 7A. The magnitude of the decrease of the DTA effect becomes substantial with high concentrations of the finest quartz. Analysis of these data showed that in the case of a sample without a known particle size distribution of quartz, it is possible to obtain acceptable results from large particle size samples by preparing calibration curves for quartz ground to pass through a 325-mesh sieve. Similarly, with minimum grinding, passing the entire sample through the same sieve.

In order to correct differences in thermal conductivity between the test

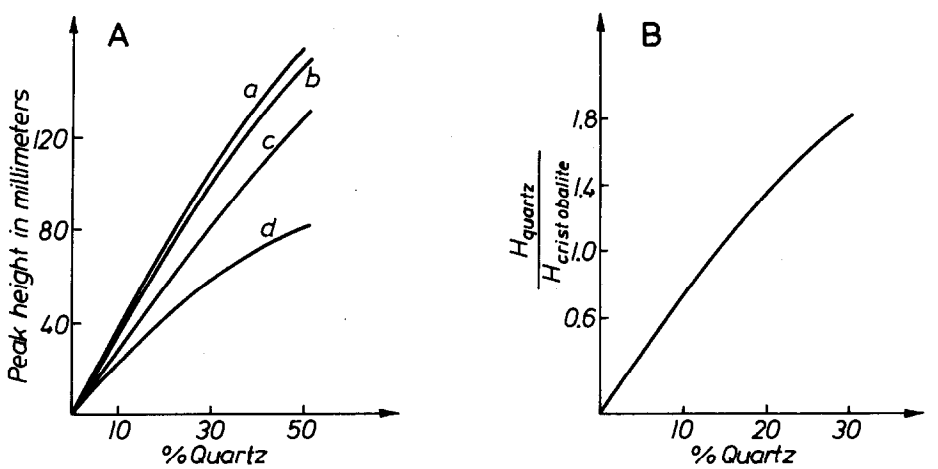

Fig. 7. (A) Relationship between the particle size of quartz and the endothermic DTA peak height of its crystal inversion (from ref. 61). Average particle size of quartz used: (a) 18.5 μm, (b) 13.5 μm, (c) 5.1 μm, and (d) 2.2 μm. Samples were diluted with silicon carbide having the same particle size. (B) Calibration curve for quartz using cristobalite as internal standard. Appropriate samples of quartz of 2.2-μm particle size, containing 5 mg of cristobalite, were diluted with silicon carbide having 400-mesh particle size. Measurements were performed using a DTA instrument. Samples (300 mg) were heated at a rate of 10 K min^{-1}, and SiC was used as reference material.

sample and inert reference material, which is necessary for accurate analysis and minimum DTA baseline drift, Weiss et al. [61] used the dilution of the test sample with a known amount of inert reference material. Aluminium oxide or silicon carbide are commonly used. The magnitude of the dilution depends on the chemical composition of the talc sample, and a sufficient dilution was achieved when 30% of the diluent was added. The addition of a diluent may prove to be the limiting factor in the DTA analysis. In the case of finer particle sizes, the thermal response of the quartz crystal inversion is considerably reduced and the addition of a large amount of diluent may cause a loss of detectability.

Also explored was the possibility of quantitative determinations of quartz in the talc samples by the standard addition or use of the internal standards method [61]. When using the former method, the added quartz must be characterized by the same size range as the average particle size range of the sample. In the latter method, a suitable compound is added to the talc sample as an internal standard. It should be thermally active at a temperature sufficiently higher or lower than that of the quartz inversion temperature so as not to affect the baseline in this region. The standard compound should preferably undergo a large, single, reversible physical change, and not to disturb sample packing or its volume. A very small amount of the standard can be used. Synthetic cristobalite was chosen for the internal standard as it gives a single reversible crystal transition into β-cristobalite at 548 K. A DTA calibration curve for quartz using cristobalite as an internal standard is shown in Fig. 7B.

Both methods appear to show promise as a means of compensating for thermal conductivity differences and matrix effects in samples of diverse chemical composition.

In order to reduce the amount of sample required for analysis, Weiss et al. [62] reported the sandwich method and micro-method for the quantitative analysis of quartz. The sandwich method involves placing a layer of inert reference material in the bottom part of the sample chamber, followed by a layer of sample surrounding the thermocouple, and a further layer of silicon carbide as an inert material on top of the sample. The micro-method allowed further reduction of the amount of material required for analysis while retaining sensitivity, by utilizing a type of holder specifically designed for very small samples, containing milligram quantities.

The results of the determinations obtained by these methods are compiled in Table 6. As can be seen, these data are in good agreement with the results of the chemical analysis [62,63]. They confirm the suitability of the DTA method for the quantitative estimation of a small amount of free, crystalline quartz in commercial talc samples. It must also be mentioned that Rowse and Jepson [64] found the DTA method to be superior compared to X-ray diffraction and classical chemical analyses, in terms of experimental precision.

TABLE 6

Analysis (wt%) of the content of free crystalline quartz in selected commercial talc samples [63]

Sample	Sandwich method	Microholder method	Prior results	
			DTA method	Chemical method
No. 2 mill				
Grade 3×	2.1	2.0	2.0	1.5
No. 3 mill				
Dust A	7.5	7.5	8.7	11.9
Grade 1 fibre	15.8	19.0	10.7	13.3
Grade 40 oil	<1.0		< 2.0	1.0
No. 6 mill				
Grade fibre	17.2	16.0	14.2	15.2
Grade 10 AC	2.3		< 2.0	1.5

Schelz [59,65] used the DTA method for the detection of chrysotile in pharmaceutical talc samples, which is a layer silicate represented by the formula $Mg_6[(OH)_8|Si_4O_{10}]$, belonging to the group of kaolinite and serpentine. The analysis of the chrysotile samples taken from 33 locations throughout the world showed that the DTA curve is characterized by the same two thermal transitions—an endothermic due to mineral dehydroxylation and an exothermic attributed to crystallization of the decomposition

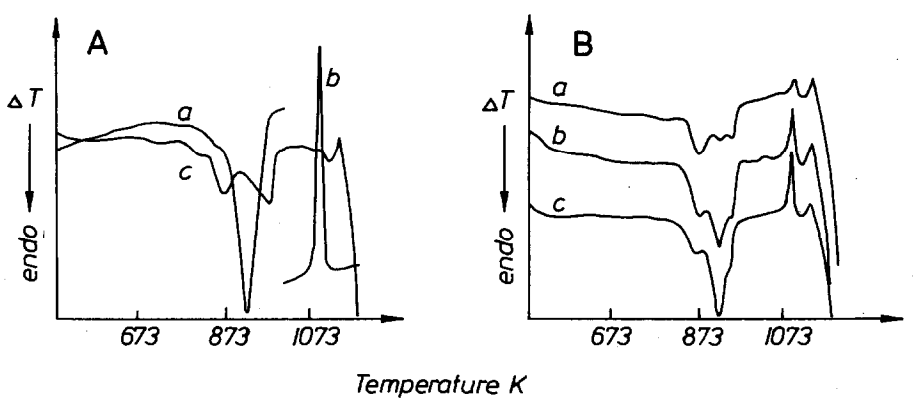

Fig. 8. (A) DTA curve of the thermal decomposition of chrysotile and talc (from ref. 65). Chrysotile was diluted with aluminia, 1:4 by weight, (a) endothermic effect of the chrysotile dehydroxylation, (b) exothermic effect of the crystallization of its decomposition products, and (c) endothermic effect of the thermal decomposition of talc containing several mineral impurities. This particular talc was selected to standard samples. (B) DTA curves of the thermal decomposition of talc samples containing: (a) 1%, (b) 3%, and (c) 5% chrysotile. Measurements were performed using an R.L. Stone DTA instrument (model LA-XYH). Samples (130–140 mg) were heated at a rate of 10 K min^{-1} in a dynamic helium atmosphere, and Al_2O_3 was used as reference material. All samples were ground to pass a 325-mesh sieve.

products [65]. This is shown in Fig. 8A. The influence of the variable contents of chrysotile in talc samples on the shape of its DTA curve is illustrated in Fig. 8B. From the figure it follows that the 1% level represents the practical limit of detection of chrysotile in pharmaceutical talc samples by this method. It has also been shown that the DTA method appears to be more sensitive than the X-ray diffraction technique, where a step-scanning procedure is used. X-ray analysis shows a 2–3% limit of detection of chrysotile because of interfering diffraction peaks of the chlorite minerals normally present in talc. By using appropriate instrumentation and carefully controlled experimental conditions, the DTA method appears to be a reliable and specific method for the detection of the presence of serpentine subgroup minerals.

Menis et al. [66], using the DTA R.L. Stone instrument, showed that the detection limit is approximately 5 μg chrysotile. On the other hand, the quantitative estimation of its content in the talc sample is possible when only a 10-mg sample contains at least 1% of chrysotile.

IDENTIFICATION OF MINERALS BASED ON DTA AND TG CURVES

Literature from around the world contains many examples of DTA [67–86] and TG [82,87–92] curves of talc samples and various other clay minerals. The analysed samples originated from locations throughout the world: U.S.S.R. [67,68,72,81,85], Germany [78–80], France [82,88], Spain [90], U.S.A. [69,70,74], Japan [73], Taiwan [77], Pakistan [83] and India [84].

The analysis of the results obtained by various authors, frequently combined with X-ray diffraction and chemical analysis, leads to a conclusion that thermoanalytical curves may be used for the rapid identification of minerals. Each sample shows a characteristic curve-shape which reflects essential differences from the curves of minerals belonging to other subgroups in the mineralogical classification.

On the DTA curves of each mineral slight fluctuations are revealed which, according to Sudo et al. [73], may be due to a combination of the dissimilarities in the particle size distribution of the mineral, differences in crystallinity, the kinds of isomorphically substituted ions, and the presence of mineral impurities in a talc sample.

Garn and Flaschen [74] showed that DTA is useful as a control tool and as a routine tool for comparing similar, but not identical, minerals. As a control tool it may be used to quickly and easily distinguish between the raw materials. The DTA method shows distinct differences in the thermal history of minerals. On the basis of the thermograms of three talc samples it has been shown that a strong endothermic effect due to dehydroxylation begins at about 1123 K. The magnitude of the peak is about the same in the case of each talc sample, but differences due to impurities make it possible to

distinguish one from another (Fig. 9A). The samples of Sierramic and Montana talcs show a small broad endothermic DTA effect around 843 K. The Sierramic talc also shows a fairly large endothermic DTA effect in the neighbourhood of 973 K. This effect occurs to a lesser extent in the Yellowstone talc.

In order to accurately interpret the thermograms, it is also advantageous to record the TG curves of the talc thermal decomposition. Langier-Kuźniarowa [82] presented simultaneously recorded DTA, TG and DTG curves of St. Barthelemy talc (Fig. 9B). X-ray diffraction studies can also be applied to enable the identification of samples having similar mineralogical composition.

Todor [92] used simultaneously recorded DTA, TG and DTG curves of the talc thermal decomposition for the quantitative determination of its mineral content. The determination is based on the TG curve between 1173 and 1373 K. An endothermic DTA effect is very useful for the estimation of the talc dehydroxylation range. The interfering accessory minerals, such as calcite and dolomite, can be removed prior to thermal analysis by shaking the sample with hydrochloric acid. Application of TG and DTG methods for

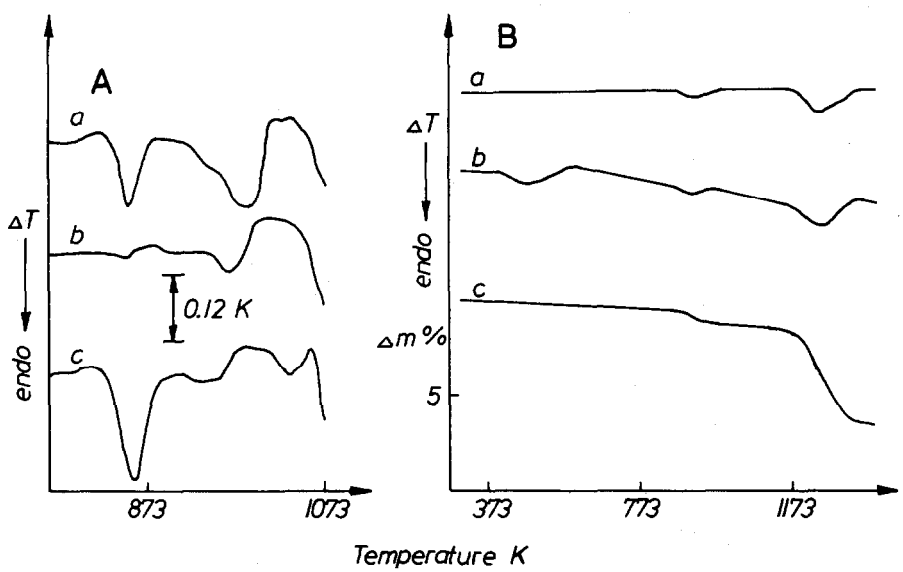

Fig. 9. (A) DTA curves of the thermal decomposition of talc samples taken from American locations: (a) Sierramic, (B) Yellowstone, and (c) Montana talc (from ref. 74). An R.L. Stone DTA instrument was used. Samples (170 mg) were heated at a rate of 10 K min^{-1} in a static air atmosphere, and α-Al_2O_3 was used as reference material. (B, a) DTG, (b) DTA, and (c) TG curves of the thermal decomposition of St. Barthelemy talc, taken from French locations (from ref. 82). Measurements were performed using a derivatograph (MOM, Hungary). Samples (752.6 mg) were heated at a rate of 10 K min^{-1} in a static air atmosphere, and α-Al_2O_3 was used as reference material.

the quality control of talc-based minerals has also been studied by Venugopal et al. [91].

Papp [93,94] applied thermoanalytical methods for the identification and semi-quantitative determination of the talc content of paper. Together with clay and calcium carbonate, talc is the most important filler. Talc in paper ash can be identified on the basis of the endothermic DTA effect at about 1223 K, and the weight loss between 1073 and 1273 K. The weight loss is proportional to the amount of talc in the paper.

It must be noted that it is possible to detect and determine many minerals as well as inorganic and organic compounds occurring in talc, on the condition that their thermal decomposition occurs at a lower temperature than that of the talc dehydroxylation. This enables simultaneous determination of talc and calcium carbonate in the paper ash [93,94], magnesite in the rocks containing talc as the contamination [95], and active components in the powders, tablets and dragees containing talc as the filling material [96].

On the margin of these problems, it must be remembered that thermoanalytical methods are used for the investigation of talc as the filling and the reinforcing agent in carbon blacks [97], for the determination of the half-decomposition times of insecticide formulations containing talc as the carrier [98], and for studies of the influence of talc on the polymorphism of spray-dried microencapsulated sulphamethoxazole [99]. Thermal methods are also used for the study of interactions between talc and a suspension of polyvinyl chloride [100], of the thermooxidative degradation of polyorganosiloxanes in the presence of talc and the other clay minerals [101], of the solid-state interactions of talc with barium carbonate [102] and cobaltous chloride [103], and for the analysis of the process of talc chlorination with gaseous chlorine at high temperatures [30].

CONCLUSIONS

From this literature review it is evident that thermoanalytical methods have found application in studies of the dehydration (the release of adsorption water which is bound to the surface of very fine grained talc samples or the release of water weakly bound by hydrogen bonding and situated between the layers of a sheet structure) as well as the dehydroxylation processes connected with degradation of the talc structure and formation of the crystalline cristobalite and magnesium metasilicate from the amorphous decomposition products of the mineral.

Moreover, the applicability of thermal methods of analysis for the detection, identification and the quantitative determination of mineral impurities which are frequently encountered in talc, e.g., quartz and chrysotile, has been proven. This is a very important problem because these materials are suspected to cause adverse effects to health. The significance of this type of

study accentuates the fact that the examination of many pharmaceutical and cosmetic talc samples normally shows a composition of only about 90% chemically pure talc [51]. The rest are mineral impurities, mostly quartz and chrysotile. On the other hand, industrial talc often contains less than 50% chemically pure talc and, therefore, represents a misuse by the world of talc. It has also been shown that in some instances industrial "talc" contains no talc but consists entirely of minerals very similar to talc, e.g., chlorite, pyrophyllite or muscovite. Thermoanalytical methods may be very useful as a tool for the control of the composition of this type of talc sample.

The examples presented do not exhaust the wide range of possibilities of application of thermoanalytical methods for the examination of layer silicates and aluminosilicates. Wider possibilities offer supplementary measurements with such tools as light microscopy, scanning and transmission electron microscopy, high-temperature X-ray diffraction, infrared spectroscopy and classical methods of chemical analysis.

It must be noted that many factors can have a significant effect on the results obtained by the thermoanalytical methods; the type of instrument influences the shape of the thermograms. For this reason, it is problematic to compare the shape of two curves recorded by different instruments. Compatible results can be obtained only when measurements are performed under similar experimental conditions (e.g., sample size, geometry of the sample holder, measuring and recording instruments) as well as assured high standardization and reproducibility analytical conditions (e.g., furnace atmosphere, particle size of the mineral powder, technique of packing the sample, inert material, and heating rate).

REFERENCES

1 M. Prużan, Technologia Środków Kosmetycznych (Technology of Cosmetic Agents), Polska Agencja Wydawnicza, Łódź, 1950, p. 75.
2 E. Rybacki and T. Stożek, Substancje Pomocnicze w Technologii Postaci Leku (Auxiliaries in Technology of Drug Formulations), PZWL, Warsaw, 1980, p. 220.
3 G. Niemczynow and J. Burchart, Mały Słownik Geologiczny (Pocket Dictionary of Geology), Wiedza Powszechna, Warsaw, 1963, p. 214.
4 I.P. Smolin, in G.O. Piloyan (Ed.), Termoanaliticheskiye Issledovaniye Sovremennykh Mineralov, Nauka, Moskow, 1970, p. 106.
5 E. Józefowicz, Chemia Nieorganiczna (Inorganic Chemistry), PWN, Warsaw, 3rd edn., 1968, p. 462.
6 W. Trzebiatowski, Chemia Nieorganiczna (Inorganic Chemistry), PWN, Warsaw, 9th edn., 1979, p. 318.
7 A. Bielański, Chemia Ogólna i Nieorganiczna (General and Inorganic Chemistry), PWN, Warsaw, 6th edn., 1979, p. 475.
8 A. Bolewski, Mineralogia Szczegółowa (Detailed Mineralogy), Wydawnictwa Geologiczne, Warsaw, 3rd edn., 1982, p. 365.
9 I.W. Gruner, Z. Kristallogr., 88 (1934) 412.

10 S.B. Hendricks, Z. Kristallogr., A, 99 (1938) 264.
11 C.W. Correns, Einführung in die Mineralogie, Springer Verlag, Berlin, 1949, p. 350.
12 B.B. Zvyagin and Z.G. Pinsker, Dokl. Acad. Nauk SSSR, 68 (1949) 505.
13 J.S. Stemple and G.W. Brindley, J. Am. Ceram. Soc., 43 (1960) 34.
14 W. Lindemann, R. Woergerbauer and H. Christenn, Sprechsaal Keram., Glas, Baustoffe, 108 (1975) 234.
15 Ch. Kiefer, C.R. Acad. Sci., Ser. C, 229 (1949) 1021.
16 Ch. Kiefer, Keram. Z., 12 (1960) 494.
17 Ch. Kiefer, Bull. Soc. Fr. Ceram., 35 (1957) 95.
18 D. Schultze, Termiczna Analiza Różnicowa (Differential Thermal Analysis), PWN, Warsaw, 1974, p. 192, (translated from German).
19 R.H. Ewell, E.N. Bunting and R.F. Geller, J. Res. Natl. Bur. Stand., 15 (1935) 551.
20 A.I. Avgustinik and V.S. Vigdergauz, Ogneupory, 13 (1948) 218.
21 A.I. Avgustinik, P.Z. Tandura and L.I. Sverchkova, Zh. Prikl. Khim. (Leningrad), 22 (1949) 1150.
22 E. Thilo and G. Rogge, Ber. Dtsch. Keram. Ges., 72 (1939) 341.
23 R.L. Stone, J. Am. Ceram. Soc., 26 (1943) 333.
24 W. Lindemann, Geol. Bl. Nordost-Bayern, 5 (1955) 143.
25 W. Lindemann, Geol. Bl. Nordost-Bayern, 6 (1956) 153.
26 W. Lindemann, Sprechsaal, 19 (1961) 508.
27 W. Krönert, H.E. Schwiete and A. Suckow, Ziegelindustrie, 17 (1964) 337.
28 W. Krönert, H.E. Schwiete and A. Suckow, Ziegelindustrie, 17 (1964) 364.
29 W. Krönert, H.E. Schwiete and A. Suckow, Naturwissenschaften, 51 (1964) 85.
30 T. Ishii, R. Furuichi and Y. Kobayashi, Thermochim. Acta, 9 (1974) 39.
31 E. Planz, Am. Ceram. Soc. Bull., 43 (1964) 443.
32 S.B. Bošković, M.Č. Gašić, V.S. Nikolić and M.M. Ristić, Proc. Br. Ceram. Soc., 10 (1968) 1.
33 J. Dereń, J. Haber and R. Pampuch, Chemia Ciała Stałego (Chemistry of the Solid State), PWN, Warsaw, 1977, p. 576.
34 M. Koltermann, Neues Jahrb. Mineral., Monatsh., 4 (1964) 97.
35 M. Koltermann, Naturwissenschaften, 51 (1964) 11.
36 M. Koltermann, Ber. Dtsch. Keram. Ges., 42 (1965) 373.
37 C.W.F.T. Pistorius, Neues Jahrb. Mineral., Monatsh., 11 (1963) 283.
38 S. Kitahara, S. Takenouchi and G.C. Kennedy, Am. J. Sci., 264 (1966) 223.
39 A.I. Avgustinik and L.I. Sverchkova, Zh. Prikl. Khim. (Leningrad), 22 (1949) 1059.
40 W. Jander, Z. Anorg. Allg. Chem., 163 (1927) 1.
41 S.B. Bošković, M.Č. Gašić, B. Živanović and M.M. Ristić, Bull. Boris Kidric Inst. Nucl. Sci., 17 (1966) 115.
42 A.M. Gistling and B.I. Brounstein, Zh. Prikl. Khim. (Leningrad), 23 (1950) 1327.
43 H. Dünwald and G. Wagner, Z. Phys. Chem., Abt. B, 24 (1934) 53.
44 C.B. Jordan and D. Duwez, J. Met., 1 (1949) 99.
45 G. Sabatier, J. Chim. Phys., 52 (1955) 60.
46 Y. Tsuzuki and K. Nagasawa, J. Earth Sci., 5 (1957) 153.
47 Y. Tsuzuki and K. Nagasawa, Kobutsugaku Zasshi, 2 (1955) 93.
48 P.G. Usov and N.V. Sobora, Izv. Tomsk. Politekh. Inst., 215 (1974) 38.
49 J.R. Ward, Gov. Rep. Announce. (U.S.), 74 (1974) 78.
50 J.A. Varela and D.C. Gillies, Ceramica (Sao Paulo), 23 (1977) 103.
51 D.H. Hamer, F.R. Rolle and J.P. Schelz, Am. Ind. Hyg. Assoc. J., 37 (1976) 296.
52 J.A. Pask and M.F. Warner, J. Am. Ceram. Soc., 37 (1954) 118.
53 L. Stoch, Pr. Mineral., Pol. Akad. Nauk, Oddzial Krakowie, Kom. Nauk Mineral., Pr. Mineral., 7 (1967) 6.

54 L. Stoch, Minerały Ilaste (Clay Minerals), Wydawnictwa Geologiczne, Warsaw, 1974, p. 119.
55 L. Stoch and Z. Stoch, in I. Buzás (Ed.), Proc. 4th Int. Conf. Therm. Anal., Budapest, 1974, Vol. 1, Akadémiai Kiadó, Budapest, Heyden, London, 1975, p. 261.
56 N.V. Andreev, Miner. Syr'e, 6 (1931) 822.
57 A. Gaweł, Przegl. Geol., 5 (1957) 299.
58 J.P. Schelz, Thermochim. Acta, 15 (1976) 17.
59 J.P. Schelz, Proc. Roundtable Discuss. Conf. Therm. Anal. Tech., DHEW (NIOSH) U.S. Publ. 1976, p. 21.
60 B. Weiss, Am. Lab., 2 (1970) 29.
61 B. Weiss, E.A. Boettner and M. Stenning, Arch. Environ. Health, 20 (1970) 37.
62 B. Weiss, K. Hosto and E.A. Boettner, Am. Ind. Hyg. Assoc. J., 34 (1973) 193.
63 E.A. Boettner, Proc. Roundtable Discuss. Am. Conf. Gov. Ind. Hyg., DHEW (NIOSH) U.S. Publ. 1973, p. 84.
64 J.B. Rowse and W.B. Jepson, J. Therm. Anal., 4 (1972) 169.
65 J.P. Schelz, Thermochim. Acta, 8 (1974) 197.
66 O. Menis, P.D. Garn and B.I. Diamondstone, in I. Buzás (Ed.), Proc. 4th Int. Conf. Therm. Anal., Budapest, 1974, Vol. 3, Akadémiai Kiadó, Budapest, Heyden, London, 1975, p. 127.
67 L.V. Ominin and F.M. Sinyakov, Miner. Syr'e, 6 (1931) 828.
68 V.P. Ivanova, Trudy Tret'ego Soveshchaniya po Eksperimentalnoyi Mineralogii i Petrografii, Inst. Geol. Nauk, Akad. Nauk SSSR, 1940, p. 116 (from Zh. Khim., 1941, Abstr. 4, No. 1, 39).
69 R.E. Grim and R.A. Rowland, Am. Mineral., 27 (1942) 746.
70 R.E. Grim and R.A. Rowland, Am. Mineral., 27 (1942) 801.
71 N.I. Gorbunov and E.A. Shurygina, Pachvoved. (Pedology), 1 (1950) 367.
72 V.S. Fadeeva and L.P. Ivanova, Tr. Issled. Tekhnol. Proizvod. Gruboi Keram., 5 (1951) 103.
73 T. Sudo, K. Nagasawa, M. Amafuji, M. Kimura, S. Honda, T. Muto and M. Tanemura, J. Geol. Soc. Jpn., 58 (1952) 115.
74 P.D. Garn and S.S. Flaschen, Anal. Chem., 29 (1957) 271.
75 O. Bolgiu and A. Dumitrescu, Acad. Repub. Pop. Rom., Stud. Cercet. Met., 2 (1957) 523.
76 H. Gelly, Met., Corros. Ind., 32 (1957) 214.
77 S. Rosenblum and P.H.H. Lu, Proc. Geol. Soc. China, 2 (1959) 147.
78 F. Lippmann, Keram. Z., 11 (1959) 475.
79 F. Lippmann, Keram. Z., 11 (1959) 524.
80 F. Lippman, Keram. Z., 11 (1959) 570.
81 V.P. Ivanova, Sredneaziatskiye Regional'nye Petrograficheskiye Soveshchaniya, Piervyi Sb., Nauka, Tashkent, 1965, p. 141 (from Zh., Geol., 1966, Abstr. No. 4, V 655).
82 A. Langier-Kuźniarowa, Termogramy Minerałów Ilastych (Thermograms of Clay Minerals), Wydawnictwa Geologiczne, Warsaw, 1967, p. 230.
83 M.A. Qaiser, M.K. Ali and A.H. Khan, Pak. J. Sci. Ind. Res., 11 (1968) 23.
84 P.K. Chatterjee, D.P. Bahl and I. Ray, Rec. Geol. Surv. India, 105 (1973) 139.
85 P.P. Smolin, B.B. Zvyagin, V.A. Drits, O.V. Sidorenko and V.A. Aleksandrova, Dokl. Akad. Nauk SSSR, 218 (1974) 924.
86 I. Soós, Muanyag Gumi, 12 (1975) 215.
87 H. Koshimizu, Sh. Higuchi and R. Otsuka, Nendo Kagaku, 21 (1981) 61.
88 H. Longchambon, Bull. Soc. Fr. Mineral., 59 (1936) 145.
89 S. Gaillére, Trans. 4th Int. Congr. Soil Sci., Amsterdam, 3 (1950) 54.
90 M. Muñoz Taboadela and V.A. Ferrandis, in R.C. Mackenzie (Ed.), The Differential Thermal Investigation of Clays, Mineralogical Society, London, 1957, p. 165.

91 J.S. Venugopal, B.V. Hirannaiah and S.K. Majumder, J. Geol. Soc. India, 23 (1982) 300.
92 D.N. Todor, Rev. Chim. (Bucharest), 25 (1974) 395.
93 J. Papp, Papiripar, 23 (1979) 175.
94 J. Papp, Sven. Papperstidn., 83 (1980) 487.
95 K. Jehan, M.A. Qaiser and A.H. Khan, J. Therm. Anal., 8 (1975) 501.
96 M. Wesołowski, Mikrochim. Acta, (1980) 199.
97 I. Soós, Kautsch. Gummi, Kunstst., 29 (1976) 619.
98 J. Espinosa de los Monteros and D. Alvarez-Estrada, Rev. Agroquim. Tecnol. Aliment., 16 (1976) 137.
99 H. Takenaka, Y. Kawashima and S.Y. Lin, J. Pharm. Sci., 70 (1981) 1256.
100 T.S. But, Sb. Tr., Vses. Nauchno-Issled. Inst. Nov. Stroit. Mater., 15 (1967) 7.
101 V.A. Krotikov, N.P. Kharitonov and G.V. Belinskaya, in A.I. Borisenko (Ed.), Temperaturoustoichivye Zashchite Pokrytiya, Trudy Seminaria po Zharostoikim Pokrytiyam, Tretyi, 1966, Nauka, Leningrad, 1968, p. 326.
102 P.G. Usov and E.P. Solomatina, Izv. Tomsk. Politekh. Inst., 174 (1971) 111.
103 M. Hassanein, Thermochim. Acta, 61 (1983) 121.